Journal of Molecular Catalysis A: Chemical 308 (2009) 114–126

Contents lists available at ScienceDirect

Journal of Molecular Catalysis A: Chemical

journal homepage: www.elsevier.com/locate/molcata

The role of glucose in abiotic humification pathways as catalyzed by birnessite

A.G. Hardie[a], J.J. Dynes[b,c], L.M. Kozak[a], P.M. Huang[a,*]

[a] Department of Soil Science, University of Saskatchewan, 51 Campus Drive, Saskatoon, SK, Canada S7N 5A8
[b] Environment Canada, 11 Innovation Place, Saskatoon, SK, Canada S7N 3H5
[c] Department of Chemistry, McMaster University, 1280 Main St. West, Hamilton, ON, Canada L8S 4M1

ARTICLE INFO

Article history:
Received 2 September 2008
Received in revised form 23 March 2009
Accepted 27 March 2009
Available online 5 April 2009

Keywords:
Abiotic humification
Polyphenol–Maillard pathway
Glucose
Glycine
Catechol
Birnessite
NEXAFS

ABSTRACT

Sugars are among the most abundant biomolecules in the environment, however, their role in abiotic humification reactions is not yet fully understood. This paper describes the effect of the molar ratio of glucose to catechol (polyphenol pathway) and glucose to catechol and glycine (integrated catechol–Maillard pathway) on humification processes and reaction products, as catalyzed by birnessite (δ-MnO_2), a ubiquitous soil mineral. Our results show that glucose enhances humification in the catechol and especially in the integrated catechol–Maillard reaction systems under the catalysis of birnessite. The visible, FTIR and NEXAFS spectroscopic data indicate that increasing the molar ratio of glucose to catechol and glycine in the integrated catechol–Maillard system enhances the formation of low-molecular weight, strongly aliphatic carboxylic Maillard reaction products in the supernatant, which are similar to natural humic acids. The NEXAFS data show that glucose also promotes the formation of carbonate ($MnCO_3$) at the expense of the aliphatic carboxylic groups in the solid residues of the birnessite-catalyzed catechol–glucose and integrated catechol–Maillard reaction systems. It is thus concluded that sugars, such as glucose, can make a significant contribution in influencing the formation and nature of humic substances and the genesis of carbonates. Our findings demonstrate the important role of sugars in affecting abiotic humification pathways and related products in natural environments.

1. Introduction

In the environment, humic substance formation is pivotal in transforming biomolecules originating from organized structures typical of organisms to randomly polymerized, heterogeneous humic substances characteristic of biogeochemical systems. The dark colour of humic substances can be attributed to oxidative browning reactions of biomolecules such as sugars, polyphenols, lipids, amino acids and proteins [1–4]. These browning reactions mostly involve carbonyl-amine reactions and result in the generation of highly coloured, high and low-molecular weight polymers [2]. Abundant research evidence at the molecular level shows that enzymes and mineral colloids can enhance the polymerization and/or polycondensation of biomolecules such as amino acids, sugars, and polyphenols, derived from the breakdown of biological residues and from biological metabolites [5–8]. Soil mineral colloids, such as metal oxides and layer silicates, have been shown to catalyze the transformations of natural and synthetic organic compounds [7]. Poorly ordered Fe- and especially Mn-oxides such as birnessite (δ-MnO_2) are the most reactive in facilitating transformations of organic compounds. This includes catalysis of the ring cleavage of polyphenols, the deamination, decarboxylation, and dealkylation of amino acids, the polymerization of phenolic compounds and their polycondensation with amino acids, and the Maillard reaction involving polycondensation of reducing sugars and amino acids [7,9–16].

Phenolics are the most widely distributed class of plant secondary metabolites and play an important role in regulating nutrient cycling in the terrestrial environment. Low-molecular weight polyphenols, such as catechol and other phenolic acids, occur universally in higher plants and are released into the soil by two principal pathways: (1) as leachate from above and below ground plant parts and (2) decomposition of above and below plant litter [17]. Another source of simple phenols is microbial metabolites [5]. The type of phenols produced during litter degradation varies substantially with the organisms involved, for instance, lignin degradation by brown-rot fungi gives rise primarily to low-molecular weight catechol-type constituents, including catechol [18]. The concentration of simple phenolics detected in soil solutions is typically low as they do not persist in soils for long due to their highly reactive nature (readily participate in polymerization and polycondensation reactions) [19,20]. For example, the concentration of water-extractable catechol from forest soils has been reported at between 2 and 8 mg kg^{-1} dry weight [21].

* Corresponding author. Tel.: +1 306 966 6838; fax: +1 306 966 6881.
E-mail address: pmh936@mail.usask.ca (P.M. Huang).

1381-1169/$ – see front matter © 2009 Elsevier B.V. All rights reserved.
doi:10.1016/j.molcata.2009.03.035

Sugars and amino acids are among the most abundant biomolecules in terrestrial and aquatic environments [22,23]. However, the role that sugars play in abiotic humification reactions is not yet fully understood. The Maillard reaction [24] is regarded as an important pathway in natural humification processes [25–27]. Even though the Maillard reaction between glucose and glycine is kinetically sluggish under normal environmental conditions [28], Jokic et al. [29] showed that birnessite substantially catalyzes the Maillard reaction under environmentally relevant conditions (25 and 45 °C at pH 7.0), resulting in the formation of humic substances very similar to that of natural humic substances. This includes the formation of amide and heterocyclic N functional groups [11]. It was shown that illumination enhances birnessite catalysis of the Maillard reaction (glucose and glycine); nonetheless it was also found that birnessite catalyzes the Maillard reaction in complete darkness [30]. Therefore, birnessite catalysis of the Maillard reaction can occur in soil or sediment environments at any depth, but the presence of sunlight should strongly accelerate the reaction. Jokic et al. [31] studied the integrated catechol–Maillard reaction system (equimolar concentrations of catechol, glucose and glycine) under environmentally relevant conditions catalyzed by birnessite, and found that the addition of catechol to the Maillard system is far more effective in promoting humification (browning) than the Maillard system alone. The influence of various polyphenols (pyrogallol and resorcinol), and their molar ratio to Maillard reagents (glucose and glycine) on humification processes as catalyzed by birnessite has also been studied [32]. The structure and functionalities of polyphenols greatly affect humification in the integrated polyphenol–Maillard reaction system. Increasing the molar ratio of polyphenols to Maillard reagents substantially enhances humification reactions and promotes the formation of humic substances with a stronger aromatic character.

Although the Maillard reaction and the influence of polyphenols on the Maillard reaction as catalyzed by birnessite (δ-MnO_2) have been reported [29–32], the role of sugars in influencing the polyphenol humification pathway and the integrated polyphenol–Maillard humification pathway as catalyzed by birnessite remains to be uncovered. Therefore, the objective of this study was to examine the effect of the molar ratio of glucose to catechol on catechol-humification processes, and the effect of the molar ratio of glucose to catechol and glycine in the integrated polyphenol–Maillard pathway on humification processes and reaction products, as catalyzed by birnessite. Catechol was selected as the model polyphenol in our reaction systems, because 1,2-dihydroxy-substituted phenolic compounds are widely occurring in nature, as they are products of lignin decomposition reactions and present in plant canopy, root leachates and microbial metabolites [5]. Glycine was selected as the model amino acid compound in this study, as it is a predominant amino acid found in soils and a major constituent of microbial cell walls [5]. Glucose was selected, as it is one of the primary decomposition products arising from the natural degradation of cellulose [23], one of the most abundant substrates in the terrestrial environment.

2. Experimental

2.1. Materials

Birnessite (δ-MnO_2) was synthesized according to a method described by McKenzie [33], which involves reducing boiling $KMnO_4$ by slowly adding concentrated HCl. The precipitate was washed by means of repeated filtration using distilled deionized water (henceforth referred to as water) on a 0.1 μm pore Millipore membrane filter, until the wash water was tested free from chloride (0.1 M $AgNO_3$ test). It was then freeze-dried and then lightly ground using a mortar and pestle. The synthesized birnessite was characterized by means of X-ray diffraction (XRD) (Rigaku Rotaflex 200SU, Tokyo, Japan), Fourier transform infrared (FTIR) spectroscopy (Bruker Equinox 55, Ettlingen, Germany), Mn L-edge near edge X-ray absorption fine structure (NEXAFS) spectroscopy on the SGM (Spherical Grating Monochromator) beamline at the Canadian Light Source (Saskatoon, SK, Canada). Catechol, D-glucose (Sigma–Aldrich ACS reagent grade >99%) and glycine (Sigma Ultra pure grade >99%) were obtained from Sigma–Aldrich Canada Ltd. (Oakville, ON, Canada). The Mn reference compounds, $MnCO_3$ (99.99%) and Mn_2O_3 (>98%) were obtained from Sigma–Aldrich (Oakville, ON, Canada) and MnO (>99.99%) and MnO_2 (>99%) from Alfa Aesar, Johnson Matthey Catalog Company, Inc. (Ward Hill, MA, USA). These were used in the Mn L-edge NEXAFS studies. International Humic Substances Society (IHSS) (St. Paul, MN, USA) Elliot soil (1S102H) and Suwannee River (1S101H) humic acid standards were used in the C K-edge NEXAFS study.

2.2. Incubation experiment

Sterile conditions were maintained throughout the experiment in order to establish the role of abiotic processes. All glassware, birnessite, water and other apparatus were autoclaved prior to the experiments. In addition to this, thimerasol, an antiseptic agent, was added to each flask (0.02%, w/v) before any of the reagents were added. Thimerasol does not affect the oxidation process of phenolic compounds [34]. The concentrations of glucose, glycine and catechol used were based on the preceding investigation of the integrated catechol–Maillard humification pathway by Jokic et al. [31], as recommended in studies of the Maillard reaction, by Hedges [35], Benzing-Purdie et al. [36], and Taguchi and Sampei [37]. The molar concentration of glucose employed in the experiments varied from one-twentieth to double that of catechol and glycine in order to investigate its impact on humic substance formation in the glucose–catechol and integrated catechol–Maillard systems. The treatments employed contained increasing amounts (0, 0.0025, 0.0250, 0.0500, 0.1000 mol) of glucose added to a fixed amount of catechol (0.05 mol) or catechol (0.05 mol) + glycine (0.05 mol) using birnessite as catalyst. Two and a half grams of birnessite was suspended in 75 mL of the reaction solutions in a 250 mL flask. There were selected control treatments in which birnessite was absent, i.e., the catechol only system (0.05 mol catechol), the glucose only system (0.05 mol glucose), the Maillard reaction system (0.05 mol glucose + 0.05 mol glycine), the catechol–glycine system (0.05 mol catechol + 0.05 mol glycine) and the integrated equimolar catechol–Maillard system (0.05 mol glucose + 0.05 mol glycine + 0.05 mol catechol). All the reaction systems were adjusted to an environmentally relevant pH 7.0 using 0.1 M HCl or 0.1 M NaOH. The final volume of the flasks was made up to 100 mL using autoclaved water.

The flasks were then tightly sealed and placed in a constant temperature water bath at 45 °C for a period of 15 days while gently shaking. Forty-five degrees centigrade is an environmentally relevant temperature as it is common in tropical and subtropical regions, and has also been reported in temperate areas as the approximate temperature of an exposed sunlit soil surface on a day when the ambient air temperature is 25 °C [38]. All treatments were performed in triplicate. The absence of microbial growth was verified by culturing aliquots of selected samples at the end of the incubation period. Aerobic microbial growth was tested for by culturing on Tryptocase Soy Agar (TSA) plates, while anaerobic microbial growth was tested for on TSA plates in a BBL GasPak 150 Large Anaerobic System. All aerobic and anaer-

obic cultures were incubated for a period of 5 and 9 days at 28 °C [31].

2.3. Characterization of reaction systems at the end of the incubation period and isolation of humic acids

At the end of the reaction period, the final Eh and pH of the suspensions were measured. The Eh was measured using an Orion combination ORP electrode (Thermo Fisher Scientific Inc., Waltham, MA), which consists of a platinum electrode with a built in calomel reference electrode and temperature probe. The sample was shaken well while still sealed and then opened and some of the suspension was decanted into a 50 mL centrifuge tube with a narrow opening. The ORP electrode was then placed immersed in the solution and then the reading was allowed to stabilize. The mV reading obtained from the pH/mV meter connected to the ORP electrode is converted to pE by the following calculation: (reading in V + standard reference half-cell potential of the calomel reference electrode in 4 M KCl at room temperature)/(0.059) [39].

The samples were then centrifuged at 25,000 × *g* for 40 min to separate the solid residue from the solution. The absorbance of the supernatant was measured between 400 and 600 nm on a UV–visible spectrophotometer (Beckman DU 650 microprocessor controlled spectrophotometer, Fullerton, CA, USA). The visible absorbance at 400 and 600 nm provides an indication of the extent of polymerization which has taken place in the reaction systems [9,10,15]. Shindo and Huang [15] studied the polymerization of polyphenols under the catalysis of short-range ordered Mn, Fe, Al and Si oxides, and showed that the yield of humic acid is directly related to the visible absorbance. Likewise, with natural humic substances, Gan et al. [40] showed that visible absorbances between 300 and 500 nm can be used to determine the concentration of fulvic acid in solution. The more aromatic and condensed the humic substances are the greater the absorption in the 600 nm range [5]. We measure the visible absorbance at 400 and 600 nm to get an indication of the extent of polymerization which has taken place. Our measurements at 400 and 600 nm are not used for calculating the E_4/E_6 ratio. To calculate E_4/E_6 ratio, the method described by Chen et al. [41] should be used, where the pH and the ionic strength are controlled. The supernatant was diluted with water prior to absorbance determination and the values obtained were subsequently multiplied by the dilution factor. The Mn content of the supernatant was determined using atomic absorption spectroscopy at 279.5 nm (Varian Spectra AA 220, Walnut Creek, CA, USA).

The solid residue was repeatedly washed with water using centrifugation at 25,000 × *g* for 40 min until the wash water was clear. These water extracts were collected and added to the supernatant. The washed residue was then freeze-dried. The combined water extracts and supernatant solution was then acidified to pH 1.0 using 6 M HCl and allowed to stand for 24 h to precipitate the humic acid (HA) fraction out of the solution [42]. The acidified suspensions were then centrifuged at 25,000 × *g* for 45 min to separate the HA fraction from the rest of the solution containing the fulvic acid (FA) fraction and non-humic substance fraction. The HA residue was then resuspended in a 0.1 M HCl and 0.3 M HF solution and shaken for 48 h to remove sorbed metals. It was then centrifuged at 25,000 × *g* for 45 min and dialyzed in 1000 Da molecular weight cut off dialysis tubing for 5–10 days in distilled deionized water until the water was tested free from chloride (0.1 M $AgNO_3$ test). The purified HA was then freeze-dried. A HA sample isolated from the supernatant of the equimolar catechol–Maillard system, without the HCl/HF treatment to remove sorbed metals, was used in the Mn L-edge NEXAFS studies to investigate the nature of Mn bonding in the HA sample.

2.4. Characterization of the solid residues and purified humic acid

2.4.1. Fourier transform infrared (FTIR) spectroscopy

FTIR spectra were obtained from the washed and freeze-dried solid residues and purified HA fractions by preparing KBr disks containing 1% (w/w) sample. The KBr disks were run on a Bruker Equinox 55 FTIR spectrometer (Ettlingen, Germany) connected with a purge gas generator.

2.4.2. Near edge X-ray absorption fine structure (NEXAFS) spectroscopy

The speciation of C and Mn was investigated in selected solid residues and supernatant HA fractions using C K-edge and Mn L-edge NEXAFS on the SGM (Spherical grating monochromator) beamline [43] at the Canadian Light Source (Saskatoon, SK, Canada). A number of pure reference Mn compounds ($MnCO_3$, MnO, Mn_2O_3, MnO_2) and IHSS soil and river HA standards, were also examined. Samples which were investigated for Mn were lightly ground and mounted on carbon tape. Samples, which were investigated for C, were mounted on gold (Au)-coated (~400 Å) silicon (Si) wafers by making dilute suspensions of the samples in distilled deionized water and then placing a droplet of the suspension on the wafer and allowing it to dry. An exit slit width of 20 μm and a dwell time of 0.3 s were used to minimize damage due to exposure to radiation. These spectra were recorded by total electron yield (TEY) at an energy step size of 0.1 eV. The Mn L-edge spectra were normalized to the TEY of a gold I_0 mesh which was fixed in front of the sample in the path of the beam. The C K-edge spectra were normalized to a clean Au-coated Si wafer, so that the signals from C in the beamline and C contamination on the gold I_0 mesh would not interfere with the signal from our samples [44]. Spectra obtained were analyzed using aXis2000 software [45]. The energy scale of the C and Mn spectra were internally calibrated using glycine and MnO, respectively, based on calibrated values reported from previous studies [46,47]. All the spectra were normalized to each other, with the maximum intensity of each spectrum fixed at one.

3. Results and discussion

In all the reaction systems studied, no aerobic or anaerobic microbial growth was observed. Thus, all the processes studied were abiotic in nature. The X-ray diffractogram of the synthesized birnessite had characteristic *d*-values at 7.21, 3.61 and 2.45 Å (diffractogram not shown) as reported by McKenzie [48]. The FTIR spectrum of the synthesized birnessite showed typical birnessite absorption bands at 3400, 1621, 509 and 466 cm^{-1} (spectrum not shown) similar to that reported by Potter and Rossman [49].

3.1. Effect of the presence of birnessite on the reaction systems

The effect of the presence of birnessite on the visible absorbance (400–600 nm) of the supernatant of the catechol–glycine, catechol–Maillard, catechol only, catechol–glucose and Maillard reaction systems is shown in Fig. 1. The presence of birnessite significantly enhanced browning (humification) in all of the reaction systems, most notably in the integrated catechol–Maillard system (Fig. 1b). Table 1 provides a summary of the solution characteristics of selected reaction systems in both the presence and absence of birnessite. The glucose only system showed the least browning both in the presence and absence of birnessite. The glucose only system in the absence of birnessite had a low final pH (5.07 ± 0.09) but no colour development (absorbance values Table 1), in contrast to the catechol only system in the absence of birnessite. The low final pH of the catechol only system in the absence of birnessite can be attributed to the oxidative polymerization (browning) reactions which result in the release of protons. It is possible that glucose

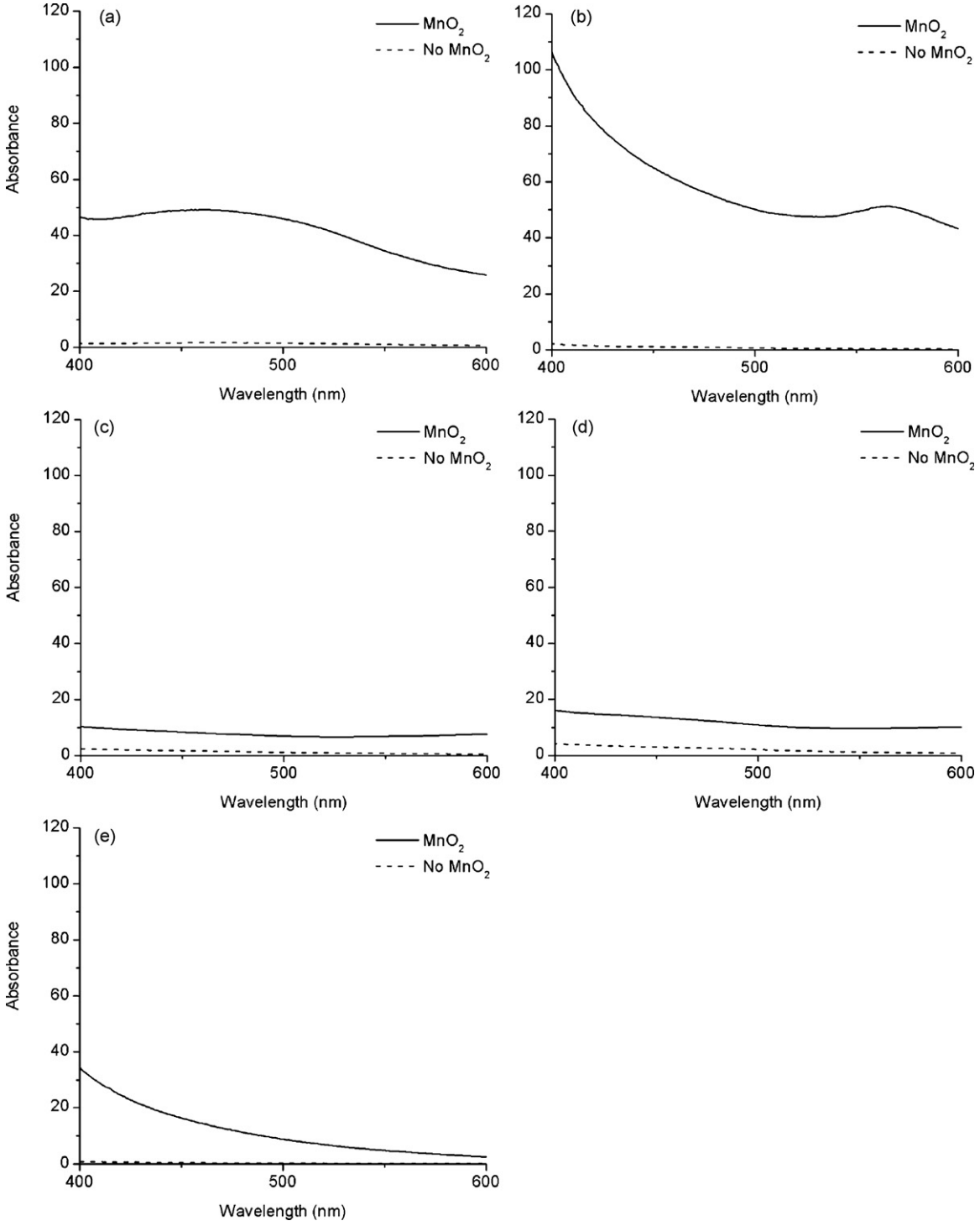

Fig. 1. The effect of the presence of birnessite on the visible absorbance (400–600 nm) of the supernatant from (a) the catechol–glycine system (0.05 mol catechol + 0.05 mol glycine), (b) the integrated catechol–Maillard system (0.05 mol catechol + 0.05 mol glucose + 0.05 mol glycine), (c) the catechol only system (0.05 mol catechol), (d) the catechol–glucose system (0.05 mol catechol + 0.05 mol glucose) and (e) the Maillard reaction (0.05 mol glucose + 0.05 mol glycine). The visible absorbances (400–600 nm) of the supernatant from the glucose only system was 0 in the absence of birnessite and ranged from 0.004 to 0.007 in the presence of birnessite (data not shown). The absorbances are scaled by the dilution factor.

underwent mild autoxidation/decomposition reactions at 45 °C (glucose autoxidation readily occurs at low temperatures, such as under physiological conditions as in the case of diabetes). This could lead to the formation of organic acids, carbonyl compounds and the release of CO_2 [50,51] which would contribute to the lowering of the final pH of the system but would not necessarily contribute to colour formation.

The addition of glucose to catechol (compare the visible absorbance of the catechol only system with that of the catechol–glucose system) resulted in a substantial enhancement in the browning in the presence of birnessite (Table 1). This is attributable to the reaction of catechol with glucose dehydration, oxidation, and aromatization derivatives catalyzed by birnessite. Likewise, the addition of glucose to the catechol–glycine system

Table 1
Comparison of the effect of the presence of birnessite on the visible absorbance, pH and redox potential (pH + pE), and Mn concentration of the supernatant of selected reaction systems.

Treatment[a]	Visible absorbance		pH	pH + pE	Mn (mmol L^{-1})
	400 nm	600 nm			
Presence of birnessite					
Catechol	10.29 ± 4.21	6.97 ± 4.06	7.27 ± 0.04	8.59 ± 0.12	17.3 ± 0.2
Catechol–glycine	55.92 ± 6.91	31.58 ± 5.54	7.13 ± 0.12	7.54 ± 0.86	31.6 ± 4.6
Catechol–glycine–glucose	100.59 ± 6.37	44.21 ± 5.34	6.85 ± 0.01	6.74 ± 0.19	92.0 ± 4.9
Catechol–glucose	15.65 ± 0.45	10.63 ± 0.25	6.80 ± 0.18	6.88 ± 0.13	19.7 ± 0.8
Glucose only	0.07 ± 0.02	0.04 ± 0.01	7.49 ± 0.22	12.80 ± 0.92	13.3 ± 2.4
Absence of birnessite					
Catechol	2.04 ± 0.33	0.62 ± 0.26	4.17 ± 0.29	10.45 ± 0.72	–
Catechol–glycine	1.71 ± 0.75	0.78 ± 0.16	6.52 ± 0.04	9.91 ± 0.40	–
Catechol–glycine–glucose	2.84 ± 0.57	0.42 ± 0.09	5.49 ± 0.07	8.78 ± 0.52	–
Catechol–glucose	3.12 ± 1.13	0.38 ± 0.41	3.93 ± 0.15	10.67 ± 0.31	–
Glucose only	0	0	5.07 ± 0.09	11.56 ± 0.25	–

[a] Amount of each reagent added was 0.05 mol in the reaction systems.

substantially enhanced browning in the presence of birnessite. The addition of glycine to catechol also significantly enhanced browning reactions in the presence of birnessite, but not in the absence of birnessite.

The pH + pE value is a function of the dissolved oxygen concentration in solution, and is thus an indication of the redox status of a system [52]. The addition of glucose to the catechol or catechol–glycine system in the presence of birnessite consistently decreased the pH and the pH + pE (Table 1), indicating the generation of more protons and consumption of more oxygen. This is in accord with the enhancement of the absorbance at both 400 and 600 nm with the addition of glucose to the catechol or catechol–glycine system (Fig. 1). Except for the glucose only system, the systems reacted in the presence of birnessite had lower final redox status (pH + pE) values than in the absence of birnessite (Table 1), which indicates more oxygen was consumed and thus oxidative polymerization reactions were enhanced. Systems reacted in the presence of birnessite also had higher final pH values, as a result of the reductive dissolution of birnessite by the biomolecules which results in the consumption of protons.

3.2. Influence of the molar ratio of glucose to catechol with or without glycine on reaction systems reacted in the presence of birnessite

The effect of the molar ratio of glucose to glycine and catechol in the integrated catechol–Maillard system, and that of glucose to catechol in the catechol–glucose system, on the visible absorbance of the supernatant at 400 and 600 nm is shown in Fig. 2. Increasing the molar ratio of glucose to catechol and glycine in the catechol–Maillard system resulted in a substantial increase in the visible absorbance of the supernatant at 400 nm (Fig. 2a) but not to the same extent at 600 nm (Fig. 2b). This indicates that increasing the molar ratio of glucose to catechol and glycine in the integrated catechol–Maillard reaction system enhanced the formation of lower molecular weight humic polymers. This is attributable to the enhanced formation of Maillard reaction products which are relatively lower molecular weight products as indicated by the higher visible absorbance of the supernatant of the Maillard reaction system at lower wavelengths (~400 nm), compared with that at higher wavelengths (~600 nm) (Fig. 1e).

Increasing the molar ratio of glucose to catechol resulted in an increase in the visible absorbance at both 400 and 600 nm (Fig. 2). Therefore, adding increasing amounts of glucose to catechol enhanced browning reactions but to a lesser extent than in the integrated catechol–Maillard system. The absorbance results (Fig. 2) also indicate the important role that glycine plays in enhancing browning reactions; glycine readily undergoes polycondensation with polyphenols such as catechol or reducing sugars such as glucose in the presence of birnessite to form darkly coloured polymers [10,29,53–55].

The effect of the molar ratio of glucose to glycine and catechol in the integrated catechol–Maillard system, and that of glucose to catechol in the catechol–glucose system, on the final pH and Mn

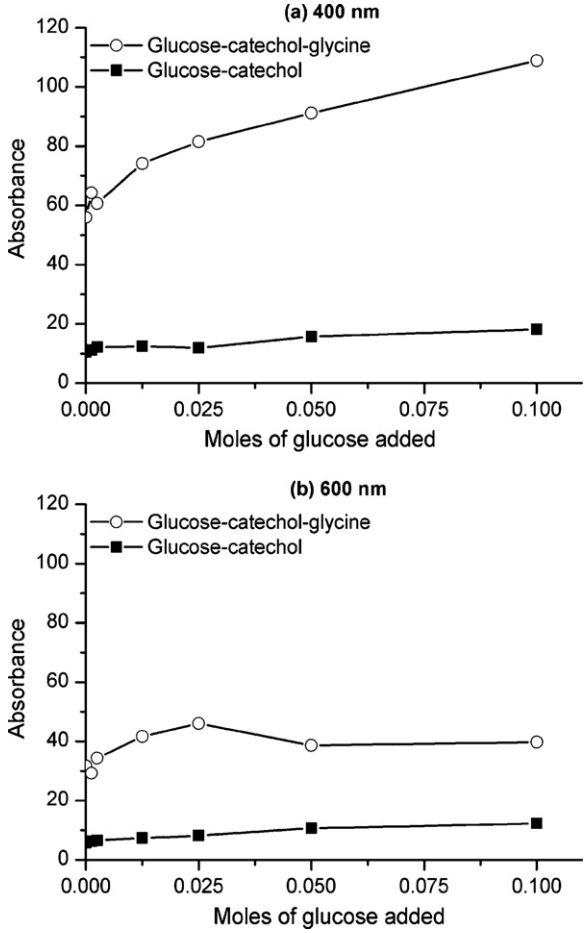

Fig. 2. Comparison of the absorbances of the supernatants at (a) 400 and (b) 600 nm of the integrated catechol–Maillard (0.05 mol catechol + 0.05 mol glycine + varying mole glucose) and glucose–catechol (0.05 mol catechol + varying mole glucose) systems reacted in the presence of birnessite with increasing amount of glucose added to the system. The absorbances are scaled by the dilution factor.

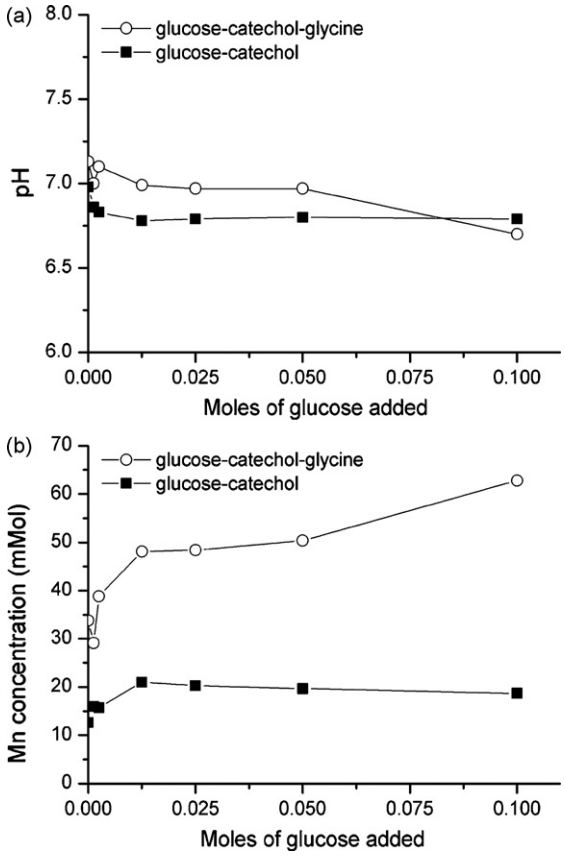

Fig. 3. Comparison of (a) the final pH and (b) the Mn concentration of the supernatant of the integrated catechol–Maillard (0.05 mol catechol + 0.05 mol glycine + varying mole glucose) and glucose–catechol (0.05 mol catechol + varying mole glucose) reaction systems catalyzed by birnessite, with increasing amount of glucose added.

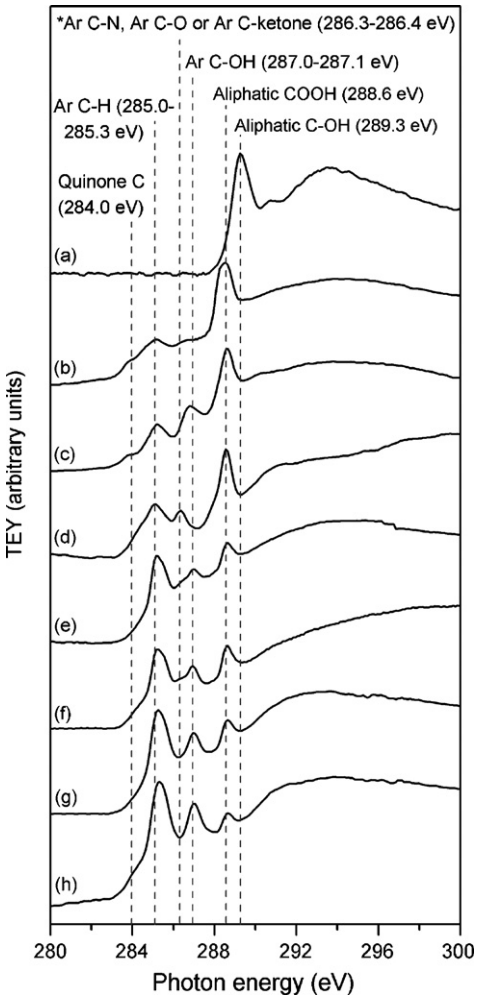

Fig. 4. Carbon K-edge NEXAFS spectra of (a) unreacted glucose, the IHSS (b) soil and (c) river humic acids, and the HA extracted from the supernatants of systems reacted in the presence of birnessite: (d) the Maillard reaction system (0.05 mol glucose + 0.05 mol glycine); the integrated catechol–Maillard reaction system (0.05 mol catechol + 0.05 mole glycine) with: (e) 0.1 mol glucose, (f) 0.05 mol glucose, (g) 0.025 mol glucose; and (h) the catechol and glycine reaction system (0.05 mol catechol + 0.05 mol glycine). *Ar = aromatic.

concentration of the supernatants is shown in Fig. 3. The pH of the reaction systems is controlled by two dominant processes: (i) the proton-consuming reduction of birnessite (Eq. (1)), and (ii) the proton-generating oxidative polymerization reactions of hydroxylated aromatic compounds, such as catechol (Eq. (2)) [56].

$$MnO_2 + 4H^+ + 2e^- \rightarrow Mn^{2+} + 2H_2O \quad (1)$$

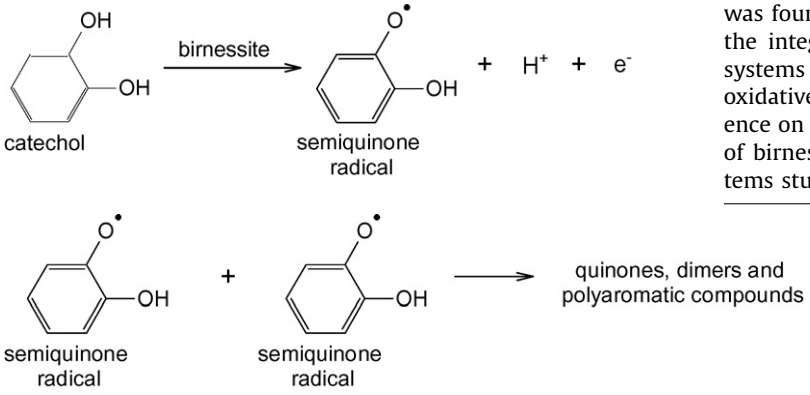

(2)

Polycondensation reactions, such as the condensation of glucose and glycine [57] or the dehydration of glucose to form hydroxymethylfurfural [58], result in the release of H_2O and thus do not affect the pH of the system. However, oxidative polymerization reactions of hydroxylated aromatic compounds, e.g. polyphenols, and other reactive aromatic compounds (furfural and hydroxymethylfurfural compounds) generated by the Maillard reaction or dehydration of glucose [25,58–61] would generate protons. It was found that birnessite was completely dissolved (reduced) in the integrated catechol–Maillard and catechol–glucose reaction systems (FTIR data shown later). This means that the extent of oxidative polymerization reactions would have a greater influence on the net final pH of reaction systems than the dissolution of birnessite, which occurred to the same extent in all the systems studied. Increasing the amount of glucose in the integrated catechol–Maillard system resulted in a decrease in the pH value of the system, indicating that glucose enhanced oxidative polymerization reactions. However, increasing the amount of glucose in the catechol–glucose system only resulted in an initial decrease in the pH of the system (Fig. 3a), indicating that glucose only slightly enhanced oxidative polymerization reactions in the catechol–glucose system.

Increasing the concentration of glucose in the integrated catechol–Maillard system resulted in a substantial increase in the Mn concentration in the supernatant (Fig. 3b). However, increasing the amount of glucose in the catechol–glucose system resulted in an initial increase (up to 0.0025 mol glucose added), but then the Mn concentration tended to level off in the supernatant (Fig. 3b). As all the birnessite in the reaction systems was dissolved, the complexation of Mn(II) by humic products and the formation of Mn(II) phases such as $MnCO_3$ in the reaction systems controls the amount of Mn in solution. This will be discussed in further detail in the next section.

3.3. Characterization of reaction products from systems reacted in the presence of birnessite

3.3.1. Humic acid isolated from the supernatant

3.3.1.1. Carbon K-edge NEXAFS spectroscopy. The C K-edge NEXAFS spectra of the HA isolated from the supernatant of selected reaction systems, unreacted glucose, and natural IHSS soil and river HA standards are shown in Fig. 4. Spectroscopic assignments are based on the absorption maxima of the reference compounds (glucose, glycine and pyrogallol) and on values reported by previous C NEXAFS studies [62–66]. The NEXAFS narrower and sharper core (C 1s) $\rightarrow \pi^*$ transitions have been found to be the most useful for chemical analyses and identification of organic compounds due to their chemical sensitivity based on the chemical energy shifts [62].

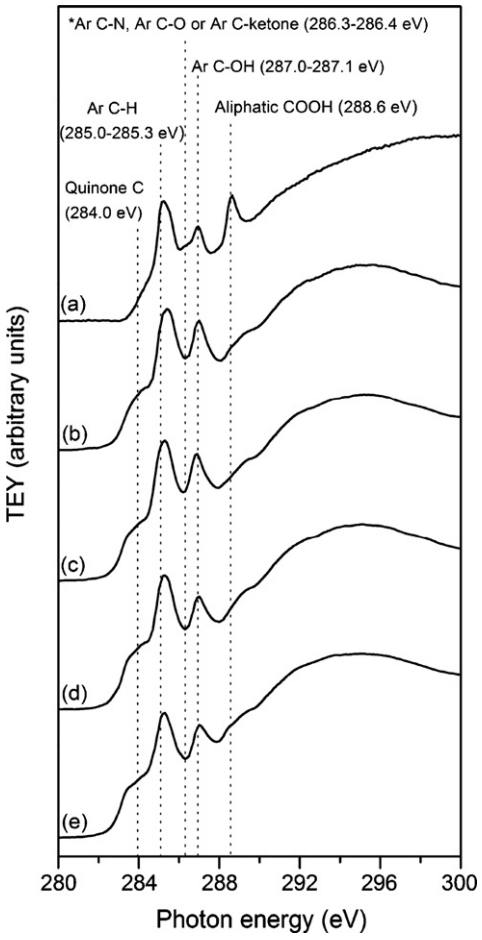

Fig. 5. Carbon K-edge NEXAFS spectra of the HA extracted from the supernatants of systems reacted in the presence of birnessite: (a) the integrated equimolar catechol–Maillard reaction (0.05 mol catechol + 0.05 mol glucose + 0.05 molm glycine); the catechol-glucose reaction system (0.05 mol catechol) with (b) 0.1 mol glucose, (c) 0.05 mol glucose, (d) 0.025 mol glucose; and (e) the catechol only system (0.05 mole catechol). *Ar = aromatic.

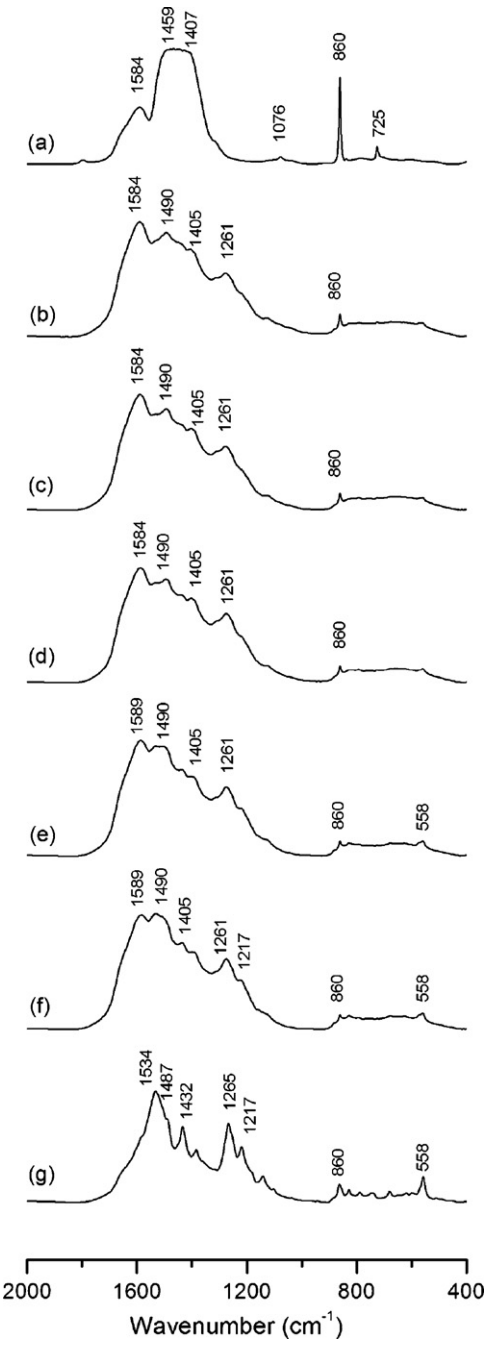

Fig. 6. FTIR spectra of the solid residues isolated from the reaction systems catalyzed by birnessite: (a) the Maillard reaction; integrated catechol–Maillard reaction systems with: (b) 0.1 mol glucose, (c) 0.05 mol glucose, (d) 0.025 mol glucose and (e) 0.0025 mol glucose; (f) the catechol–glycine system (0.05 mol catechol + 0.05 mol glycine); and (g) the catechol only system (0.05 mol catechol).

The lowest absorption bands at around 284.0 eV usually correspond to molecules with low energy π^* states, such as quinones [67]. Absorption bands near 285 eV are generally ascribed to C 1s (C–H) $\rightarrow 1\pi^*_{C=C}$ transitions [62,64], which are characteristic of C=C unsaturation. The transitions of aromatic C bound to carbonyl (e.g., terephthalate species) tend to overlap with unsaturated aromatic C–H transitions due to the strong electronic interactions between the benzene π^* density and carbonyl π^* density, and are generally found in the 284.4–285.0 eV range [64]. The absorption bands near 286–288 eV are characteristic of functionalized aromatic groups C 1s (C–R) $\rightarrow 1\pi^*_{C=C}$ transitions (R = functional group), such as aromatic C bound to aldehyde (286.0 eV), ketone (286.4 eV), urea

(286.4 eV), carbamate (286.6–286.8 eV), amine (286.8–286.9 eV), phenol (287.0–287.3 eV) and ester (287.1 eV) groups [62–65]. Heterocyclic N compounds C 1s (C–N) → $1\pi^*_{C=C}$ transitions also occur in the ~286–287 eV range, e.g., pyridine (285.7 eV) and pyrrole (286.3 eV) [63,65]. The C=N and C≡N π^* transitions usually occur around 286.3 eV [66]. Generally speaking, a stronger electron withdrawing substituent on the aromatic ring will result in a higher energy shift of the C 1s (C–R) → $1\pi^*_{C=C}$ transition.

The carbonyl C 1s (C–R) → $1\pi^*_{C=O}$ transitions usually occur between 286 and 291 eV, and can be used to distinguish between groups such as aldehydes (286.2–286.4 eV), ketones (286.6–286.8 eV), amide (287.8–288.2 eV), acetic/acetate (288.1–288.6 eV), urea (289.2–289.8 eV), carbamate (289.9–290.1 eV) and carbonate (290.2–290.6 eV) [62]. The main cause of the shifts observed in C 1s (C–R) → $1\pi^*_{C=O}$ transitions is the inductive effect of the neighbouring atoms on the carbonyl C 1s binding energy [62]. Low lying σ^* orbitals also provide valuable information in identifying aliphatic functionalities. Saturated aliphatic C exhibits C 1s (C–H) → σ^*_{C-H} transitions in the 287.1–287.9 eV range, while aliphatic alcohol C 1s (C–H) → σ^*_{C-O} transitions are found shifted to a higher energy in the 289.2–289.5 eV range [63].

The C K-edge spectrum of the unreacted glucose shows the dominant functional group of glucose which is the aliphatic alcohol group (289.3 eV). It is interesting to note that aliphatic alcohol functional group is not evident in the spectra of the natural IHSS HA samples (Fig. 4b and c) nor the HA isolated from glucose containing reactions systems (Fig. 4d–g). This indicates that glucose is completely transformed during the humification reactions. The IHSS natural soil and river HA (Fig. 4b and c) were dominated by aliphatic carboxylic functionalities (288.6 eV), and also contained quinone C (284.0 eV), aromatic C–H (285.0–285.3 eV), and functionalized aromatic C, such as aromatic C bound to N, O or ketone, and phenolic groups (286.4–287.1 eV). The HA isolated from the supernatant of the Maillard reaction system (Fig. 4d) was also strongly aliphatic carboxylic (288.6 eV) in nature, and contained aromatic C–H (285.0–285.3 eV) and aromatic C bound to N, O, ketone or hydroxyl groups (286.4–287.1 eV). In the catechol–glycine system (Fig. 4h), the HA isolated from the supernatant was dominated by aromatic C–H (285.0–285.3 eV) and phenolic groups (287.0–287.1 eV), and contained a relatively smaller amount of aliphatic carboxylic groups (288.6 eV) than the integrated catechol–Maillard systems (Fig. 4e–g). The addition of glucose (0.025 mmol) to the catechol–glycine system (Fig. 4g) significantly enhanced the relative intensity of the aliphatic carboxylic group peak (288.6 eV). Increasing the molar ratio of glucose to catechol and glycine in the integrated catechol–Maillard system (Fig. 4g–e) promoted the formation of aliphatic carboxylic (288.6 eV) and aromatic C bound to N, O or ketone groups (286.3–286.4 eV), which are similar to the functionalities observed in the Maillard reaction system HA (Fig. 4d) and the natural HAs (Fig. 4b and c).

The C K-edge NEXAFS spectra of the HA isolated from the supernatant of selected catechol–glucose reaction systems is shown in Fig. 5. In comparison to the HA from the integrated equimolar catechol–Maillard system (Fig. 5a), the HA from the catechol–glucose systems (Fig. 5b– d) and catechol only (Fig. 5e) contained very little aliphatic carboxylic groups (288.6 eV). Furthermore, the spectra of the HA from catechol–glucose systems (Fig. 5b–d) were very similar to that of the catechol only system (Fig. 5e), regardless of the amount of glucose added to the system. There appears to be a slight increase in the relative intensity of the phenolic group peak (287.0–287.1 eV) in the HA from catechol–glucose systems with high amounts of glucose (0.05 and 0.1 mol glucose) (Fig. 5b and c) compared to the HA from the catechol–glucose system with 0.025 mol glucose and the catechol only system (Fig. 5d and e).

It can be concluded from the C K-edge spectra in Figs. 4 and 5, that it is the reaction of glucose and glycine (i.e., the Maillard reaction) in the integrated catechol–Maillard system (Figs. 4d–f and 5a) that significantly promotes the formation of aliphatic carboxylic functional groups in the HA fraction isolated from the supernatant. The HA from the catechol–glycine system (Fig. 4h) and glucose–catechol systems (Fig. 5b–d) did not contain relatively as high amounts of aliphatic carboxylic functional groups as the HA from the integrated catechol–Maillard systems. It can be further concluded that increasing the molar ratio of glucose to catechol and glycine in the integrated catechol–Maillard system (Fig. 4g–d) promoted the formation of Maillard reaction-type functional groups (aliphatic carboxylic and aromatic C bound to N, O or ketone functional groups) (Fig. 4c) in the HA fraction isolated from the supernatant of the reactions systems.

3.3.2. Solid phase

3.3.2.1. FTIR spectroscopy. The FTIR spectra of the solid residues from the catechol–glycine and selected integrated catechol–Maillard systems catalyzed by birnessite are shown in Fig. 6. Comprehensive assignment of the absorption bands

Table 2
Assignments of FTIR absorption bands of the solid residues of the Maillard reaction, integrated catechol–Maillard, catechol–glycine and catechol only systems shown in Fig. 6.

(a) Maillard reaction system		(b)–(e) Integrated catechol–Maillard and (f) catechol–glycine systems		(g) Catechol only system	
Wavenumber (cm^{-1})		Wavenumber (cm^{-1})		Wavenumber (cm^{-1})	
725	Mn carbonate C–O out of plane bend	558	Mn–O vibrations, aliphatic C–O stretches	558	Mn–O vibrations
860	Mn carbonate C–O stretch	860	Mn carbonate C–O stretch	860	Mn carbonate C–O stretch
1076	Mn carbonate C–O stretch	1217	C–O stretch of phenols or phenyl ethers	1217	C–O stretch of phenols or phenyl ethers
1407	OH deformation of phenols, C–H deformation of CH_2 and CH_3, symmetrical stretch of COO^-	1261	C–O stretch of phenols and phenyl ethers	1265	C–O stretch of phenols or phenyl ethers
1459	Mn carbonate symmetric C–O stretch, assymetrical bending of CH_2 and CH_3 deformation band	1405	OH deformation of phenols, C–H deformation of CH_2 and CH_3, symmetrical stretch of COO^-	1432	Mn carbonate symmetric C–O stretch, OH deformation of phenols, C–H deformation of CH_2 and CH_3, symmetrical stretch of COO^-
1584	Aromatic C=C stretch, Symmetric C–O stretch of COO^-, N–H deformation + C=N amide II band	1490	Symmetric C-O stretch of COO^-, N-H deformation + C=N amide II band	1487	Symmetric C–O stretch of COO^-
3400	OH stretch	1584–1589	Aromatic C=C stretch, symmetric C–O stretch of COO^-, N–H deformation + C=N amide II band	1534	Aromatic C=C stretch, symmetric C–O stretch of COO^-
		3340–3400	OH stretch	3390	OH stretch

+ The spectra from 2000 to 4000 cm^{-1} are not shown in Fig. 6.

in Fig. 6 is given in Table 2. Interpretation of the absorption bands was based on the spectra of the reference compounds ($MnCO_3$, birnessite, catechol, glucose and glycine) and previous works [5,68–71]. The broad OH stretch absorption band at around 3340–3400 cm^{-1} observed in all the spectra (Fig. 6), Table 2 is also attributed to intramolecular H-bonding between polymers [69]. The solid residue from the Maillard reaction (Fig. 6a) consisted predominantly of rhodochrosite ($MnCO_3$) as indicated by the absorbance bands at 725, 860, 1076 and 1459 cm^{-1} [71]. Increasing the molar ratio of glucose to catechol and glycine in the integrated catechol–Maillard reaction system resulted in an increase in $MnCO_3$ in the solid residues as indicated by the relative intensity of the carbonate C–O stretch at 860 cm^{-1} (Fig. 6f–b). There was also a subsequent decrease in the relative intensity of the absorbance band at 1490 cm^{-1}, which indicates a decrease in carboxylic or amide groups (Fig. 6f–b).

The FTIR spectra of the solid residues from the catechol only, selected catechol–glucose systems, and glucose only system,

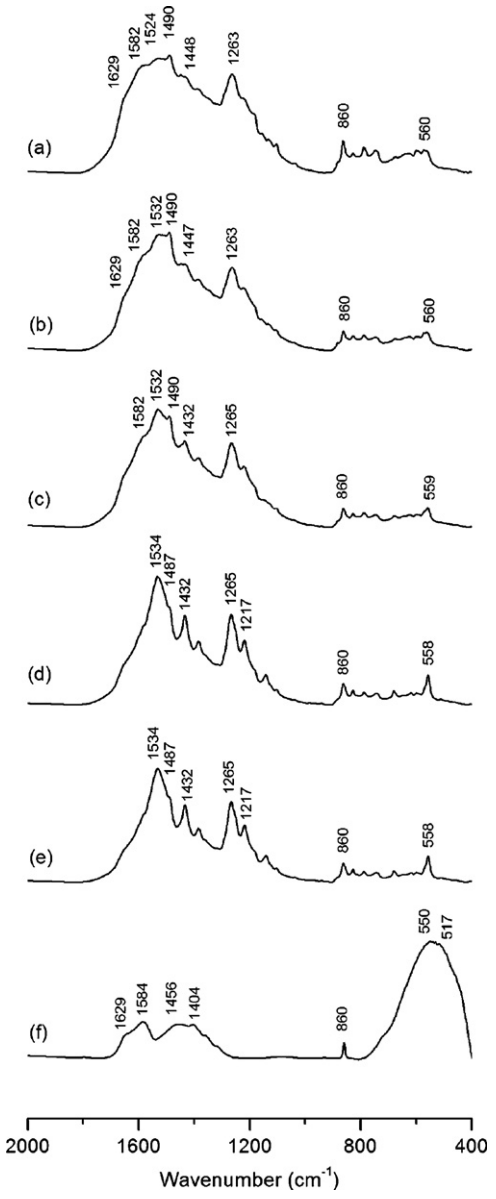

Fig. 7. FTIR spectra of the solid residues isolated from the reaction systems catalyzed by birnessite: the catechol–glucose reaction systems with: (a) 0.1 mol glucose, (b) 0.05 mol glucose, (c) 0.025 mol glucose and (d) 0.0025 mol glucose; (e) the catechol only system (0.05 mol catechol); and (f) the glucose only system (0.05 mol glucose).

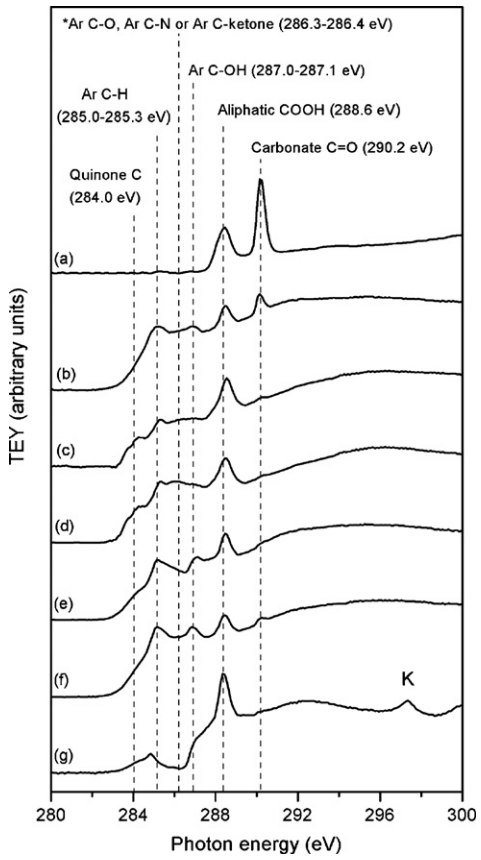

Fig. 8. Carbon K-edge NEXAFS spectra of the solid residues from selected systems reacted in the presence of birnessite: (a) the Maillard reaction (0.05 mol glucose + 0.05 mol glycine); the integrated catechol–Maillard system with (b) 0.1 mol glucose, and (c) 0.05 mol glucose; (d) the 0.05 mole catechol only system; the catechol–glucose system with (e) 0.05 mol glucose, and (f) 0.1 mol glucose; and (g) the 0.05 mol glucose only system. *Ar = aromatic.

reacted in the presence of birnessite, are shown in Fig. 7. Comprehensive assignment of the absorption bands in Fig. 7 is given in Table 3. Similar to the integrated catechol–Maillard system (Fig. 6), increasing the amount of glucose in the catechol–glucose system increased the amount of $MnCO_3$ (860 cm^{-1}) in the solid phase (Fig. 7e–a), particularly in the catechol–glucose system with 0.1 mol glucose (Fig. 7a). Increasing the molar ratio of glucose to catechol also resulted in an increase in the relative intensity of the absorption bands at 1448, 1582 and 1629 cm^{-1}, which are quite similar to the absorption bands observed in the glucose only system, i.e., 1456, 1584 and 1629 cm^{-1}. These bands are attributed to carbonate C–O stretches (1432–1456 cm^{-1}), phenol O–H stretches (1432–1448 cm^{-1}), aliphatic C–H stretches (1432–1456 cm^{-1}), COO^- stretches (1432–1448 and 1582–1584 cm^{-1}) and, in particular, aromatic C=C stretches (1584 and 1629 cm^{-1}). In contrast to the other reaction systems, the solid residue of the glucose only system (Fig. 7f) contained birnessite (517, 550 cm^{-1}), $MnCO_3$ (865, 1456 cm^{-1}) and organics (1404, 1456, 1584, 1629 cm^{-1}). The presence of birnessite in the solid phase of the glucose only system was confirmed by XRD (the *d*-values of 7.21 and 2.14 Å, diffractogram not shown). This means that glucose alone was not able to completely reduce the birnessite, unlike the other reaction systems.

3.3.2.2. Carbon K-edge NEXAFS spectroscopy. The C K-edge NEXAFS spectra of the solid residues from the Maillard reaction, selected integrated catechol–Maillard, catechol–glucose, catechol only and glucose only systems, reacted in the presence of birnessite are shown in Fig. 8. All the spectra show the strong presence of aliphatic

Table 3
Assignments of FTIR absorption bands of the solid residues of the catechol–glucose, catechol only and glucose only systems shown in Fig. 7.

(a), (b) and (c) Catechol–glucose system with 0.1, 0.05 and 0.025 mol glucose, respectively		(d) Catechol–glucose system with 0.0025 mol glucose and (e) catechol only system		(f) Glucose only system	
Wavenumber (cm^{-1})		Wavenumber (cm^{-1})		Wavenumber (cm^{-1})	
559–560	Mn–O vibrations, aliphatic C–O stretches	558	Mn–O vibrations, aliphatic C–O stretches	517, 550	Mn–O vibrations (birnessite and other Mn(III)/(IV) oxides
860	Mn carbonate C–O stretch	860	Mn carbonate C–O stretch	860	Mn carbonate C–O stretch
1263–1265	C–O stretch of phenols or phenyl ethers	1217	C–O stretch of phenols or phenyl ethers	1404	OH deformation of phenols, C–H deformation of CH_2 and CH_3, symmetrical stretch of COO^-
1432–1448	Mn carbonate symmetric C–O stretch, OH deformation of phenols, C–H deformation of CH_2 and CH_3, symmetrical stretch of COO^-	1265	C–O stretch of phenols or phenyl ethers	1456	Mn carbonate symmetric C–O stretch, assymetrical bending of CH_2 and CH_3 deformation band
1490	Symmetric C–O stretch of COO^-	1432	Mn carbonate symmetric C–O stretch, OH deformation of phenols, C–H deformation of CH_2 and CH_3, symmetrical stretch of COO^-	1584	Aromatic C=C stretch, Symmetric C–O stretch of COO^-, N–H deformation + C=N amide II band
1524–1532	Aromatic C=C stretch, Symmetric C–O stretch of COO^-	1487	Symmetric C–O stretch of COO^-	1629	Aromatic C=C stretch
1582	Aromatic C=C stretch, symmetric C–O stretch of COO^-, N–H deformation + C=N amide II band	1534	Aromatic C=C stretch, Symmetric C–O stretch of COO^-	3400	OH stretch
1629	Aromatic C=C stretch	3390	OH stretch		
3400	OH stretch				

+ The spectra from 2000 to 4000 cm^{-1} are not shown in Fig. 7.

carboxylic groups (288.6 eV), in particular the glucose only system (Fig. 8g). This is in strong contrast to the spectra of HA isolated from the supernatant of the catechol–glucose and catechol only systems (Fig. 5d–e). This is attributable to the chemical partitioning of humic products between the solution and solid phases based on the stronger relative affinity of divalent metals such as Mn(II) for carboxylic than phenolic functional groups [32,72]. Thus, there is more aliphatic carboxylic material in the solid phase than in the HA in the solution phase. There is also abundant evidence for the presence of quinone C (284.0 eV), aromatic C–H (285.0–285.3 eV) and C–OH (287.0–287.1 eV) functionalities in the solid residues (Fig. 8b–f). Although, the C K-edge spectra of the HA from the supernatant of the catechol–glucose systems did not show appreciable differences between each other as the amount of glucose was varied in the system (Fig. 5b–e), the molar ratio of glucose to catechol in the catechol–glucose system did affect the nature of the humic substances in the solid residues (Fig. 8d–f). Increasing the amount of glucose in the catechol–glucose and integrated catechol–Maillard systems decreased the formation of quinone C (284.0 eV); in contrast the formation of aromatic C–H (285.0–285.3 eV) and aromatic C–OH (287.0–287.1 eV) was enhanced by increasing the amount of glucose added to the system (Fig. 8b–f).

The solid residues from the integrated catechol–Maillard and catechol–glucose systems containing 0.1 mol glucose (Fig. 8b and f) contained relatively more carbonate (290.2 eV), than the catechol–Maillard and catechol–glucose systems containing 0.05 mol glucose (Fig. 8c and e). This trend was also confirmed by FTIR spectroscopy (Figs. 6 and 7). This indicates that increasing the molar ratio of glucose to catechol or catechol and glycine in these systems enhanced the formation of $MnCO_3$. This is not related to the pH of the systems as the integrated catechol–Maillard system with 0.1 mol glucose actually had a lower pH than the integrated catechol–Maillard system containing 0.05 mol glucose (Fig. 3a). This is instead attributed to the increase in the oxidation of glucose by birnessite [73] which results in the release of CO_2 [31]. The released CO_2 is subsequently dissolved and converted to CO_3^{2-} in solution which apparently promotes the formation of $MnCO_3$.

The solid residue from the glucose only system was dominated by aliphatic carboxylic C (288.6 eV) and smaller amounts of aromatic C–H (285.0–285.3 eV) and aromatic O–H functional groups (287.0–287.1 eV) (Fig. 8g), which is supported by the FTIR data (Fig. 7f, Table 3). This is to be expected as the dominant organic products arising from the oxidation of glucose by Mn(IV) oxides are carboxylic acids [73], predominantly formic acid with minor amounts of glycolic, glyceric, and gluconic acids, as well as aromatic furfural compounds and CO_2 [60]. Lourvanij and Rorrer [58] showed that microporous clays pillared with Fe(III), Cr(III) and Al reacted with glucose at 150 °C could promote the isomerization of glucose to fructose, the partial dehydration of glucose to 5-(hydroxymethyl)-2-furaldehyde (Eq. (3)), and the cleavage of 5-(hydroxymethyl)-2-furaldehyde to form simple carboxylic acids, in particular formic acid, and CO_2 which are the final products in the reaction. They found that Fe(III), which is the strongest oxidant of the three metals investigated, was the strongest catalyst of the dehydration and cleavage of glucose to formic acid. Gonzalez and Laird [61] showed that smectites, which have both surface Lewis and Brønsted acidic sites, can catalyze the formation of hydroxymethylfurfural and furfural compounds from glucose at relatively low temperatures (37 °C). Strong acids are able to promote the dehydration of reducing sugars to form furfural compounds [74].

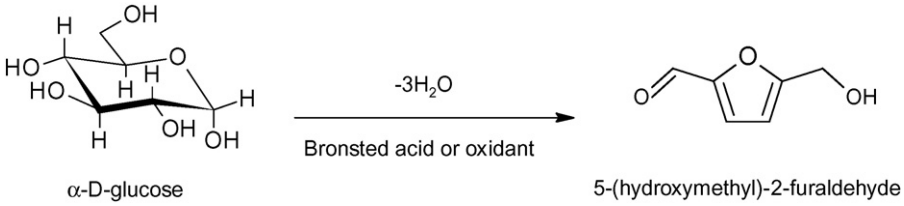

α-D-glucose 5-(hydroxymethyl)-2-furaldehyde (3)

Therefore the glucose-induced effects on the nature of the humified products in the solid residues of the catechol–glucose and integrated catechol–Maillard systems (Fig. 8b–f) are ascribed to the oxidation of glucose by Mn(IV) oxide and the resultant formation of aliphatic carboxylic groups and the aromatization products which contain aromatic C–H and –OH functional groups. The peak which appears between 296 and 298 eV in the solid residue from the glucose only system (Fig. 8g) is due to the presence of potassium [the potassium $L_{2,3}$-edge (295–300 eV) overlaps with the last part of the C K-edge] from the remaining birnessite in the residue, as shown in the FTIR data (Fig. 7f). This is because synthetic K-birnessite was used as catalyst in this study, which is synthesized from $KMnO_4$ [33].

3.3.2.3. Mn L-edge NEXAFS spectroscopy. The Mn $L_{2,3}$-edge NEXAFS spectra of the solid residues from selected reaction systems, HA from the integrated equimolar catechol–Maillard system (unpurified with HCl/HF acid, i.e., metals not removed), pure reference compounds and unreacted birnessite are shown in Fig. 9. The Mn in the solid residues from the integrated catechol–Maillard (Fig. 9a and b) and catechol–glucose (Fig. 9c and d) systems was in the Mn(II) form. By comparing the shape of the L_3-edge (638–648 eV) of the solid residues from the integrated catechol–Maillard and catechol–glucose systems (Fig. 9a–d) to that of pure $MnCO_3$ (Fig. 9g) and Mn(II) bound to humic acid (Fig. 9f), it can be deduced that the solid residues from the integrated catechol–Maillard and catechol–glucose systems contained a mixture of $MnCO_3$ and Mn(II) bound to humic products. The FTIR (Figs. 6 and 7), C K-edge NEXAFS (Fig. 8) and XRD data (diffractograms not shown) confirm the presence of $MnCO_3$ and organic products.

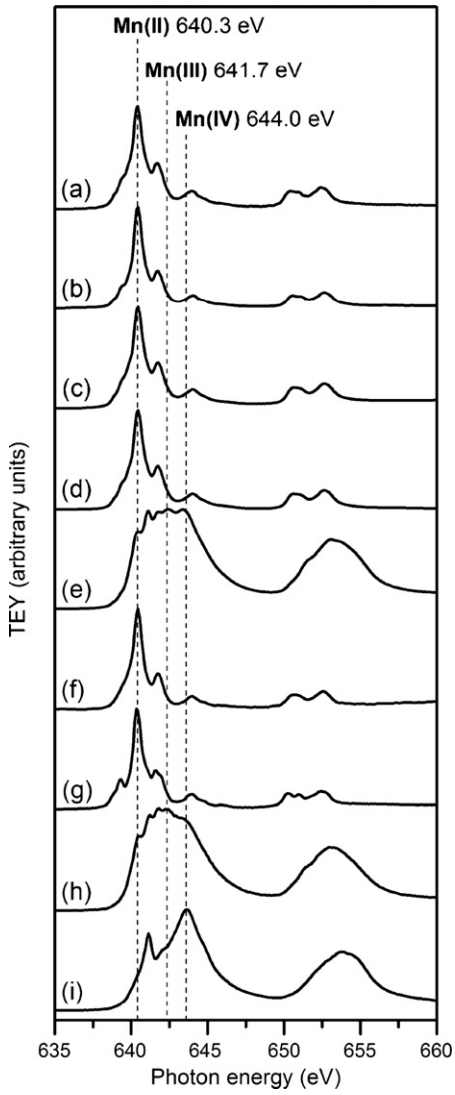

Fig. 9. Mn L-edge NEXAFS spectra of the solid residues of selected treatments reacted in the presence of birnessite: the integrated catechol-Maillard system (0.05 mol catechol + 0.05 mol glycine) with (a) 0.05 mol glucose and (b) 0.1 mol glucose added; the catechol–glucose system (0.05 mol catechol) with (c) 0.05 mol glucose and (d) 0.1 mol glucose added; (e) the 0.05 mol glucose only system; (f) unpurified HA from the integrated equimolar catechol–Maillard system; (g) pure $MnCO_3$; (h) pure Mn_2O_3 and (i) unreacted birnessite. The dotted lines indicate the photon energy of the maximum absorption peak of Mn in divalent, trivalent or tetravalent states, on the Mn L_3-edge.

The solid residue of the glucose only system (Fig. 9e) appears to contain a mixture of Mn(II), Mn(III) and Mn(IV); but judging from the overall shape of the L_3- (638–648 eV) and L_2- (650–660 eV) edges, it appears to be predominantly in the (Mn III) form (compared with the spectra of pure Mn_2O_3 – Fig. 9h). The FTIR (Fig. 7f) and C K-edge NEXAFS (Fig. 8g) spectra also confirm the presence of $MnCO_3$ and birnessite in the solid residue from the glucose only system. This shows that glucose alone was not able to reductively dissolve all of the birnessite initially added to the system, in contrast to the other systems containing catechol or catechol and glycine.

4. Conclusions

The Maillard reaction and the influence of polyphenols on the Maillard reaction as catalyzed by birnessite (δ-MnO_2) were previously reported [29–32]. However, the role of glucose in influencing the polyphenol humification pathway and the integrated polyphenol–Maillard humification pathway as catalyzed by birnessite remained to be uncovered. The results of the present study show that glucose enhanced humification (browning) reactions in the catechol and especially in the integrated catechol–Maillard reaction systems under the catalysis of birnessite. The visible absorbance data indicate that increasing the molar ratio of glucose to catechol and glycine enhanced the formation of low-molecular weight Maillard reaction products.

The C K-edge NEXAFS spectroscopic data show that glucose is completely transformed during the humification processes, as its characteristic aliphatic alcohol groups are not evident in any of the humification reaction products nor in the natural humic acids investigated. The C K-edge data show that increasing the amount of glucose in the catechol–glucose system under the catalysis of birnessite slightly enhanced the formation of aromatic C–OH functionalities and did not affect the formation of aliphatic carboxylic functional groups in the HA fraction isolated from the supernatant of the reaction systems. Increasing the amount of glucose in the integrated catechol–Maillard system under birnessite catalysis promoted the formation of Maillard reaction-type functionalities in the supernatant HA fraction, i.e., aliphatic carboxylic and aromatic C bound to N, O or ketone groups, which were similar to the functionalities observed in the natural soil and river HAs. Therefore, glucose–glycine interaction (i.e., Maillard reaction) in the integrated catechol–Maillard system is primarily responsible for the enhanced formation of the aliphatic carboxylic functionalities in the HA fraction isolated from the supernatant. It can be concluded that increasing the molar ratio of glucose to catechol and glycine in the integrated catechol–Maillard reaction system catalyzed by birnessite promoted the generally slower Maillard reaction [28], which is competing for glycine in the highly favourable polycondensation reaction between catechol and glycine [4] (Fig. 10).

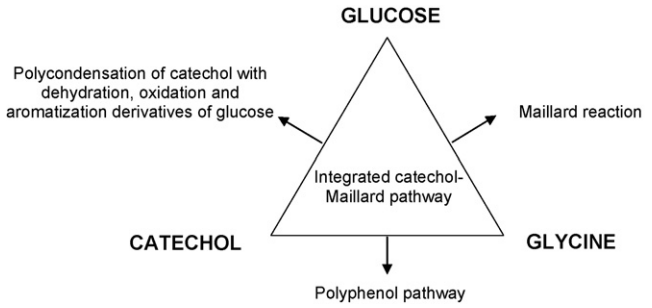

Fig. 10. Schematic representation of the various humification pathways involving glucose, glycine and catechol.

The C K-edge NEXAFS spectroscopic data of the solid residues show that increasing the amount of glucose in both the catechol–glucose and integrated catechol–Maillard reaction systems promoted the formation of aromatic C–H and aromatic C–OH but decreased the formation of quinone C and aliphatic COOH in the solid residues. Furthermore, the spectroscopic data also show that glucose promoted the formation of carbonate ($MnCO_3$) at the expense of the aliphatic carboxylic groups in the solid residues of both humification pathways. These transformations are attributable to the binary (catechol–glucose) and ternary (glucose–catechol–glycine) interactions of these biomolecules (Fig. 10). The dehydration and oxidation of glucose by birnessite results in the formation of aromatization products and also the release of CO_2 through decarboxylation and its subsequent conversion to carbonate.

It is thus concluded that sugars, such as glucose, which are one of the most abundant biomolecules in the environment, can make a significant contribution to influence the formation and nature of humic substances and the genesis of carbonates. These findings contribute to the fundamental understanding of abiotic humification reactions of biomolecules, such as sugars, polyphenols and amino acids, under the catalysis of mineral colloids, at the molecular level in soil systems. Because the nature and abundance of biomolecules substantially vary with vegetation, the findings in the present study would be useful in developing innovative land resource management strategies. This fundamental knowledge is essential to understanding humic substance formation and carbon cycling and stabilization processes in soils and sediments.

Acknowledgements

This study was supported by a Discovery Grant (GP 2383-2008-Huang) from the Natural Sciences and Engineering Research Council of Canada. We would like to thank Edwige Ottero from the Dept. Chemistry, University of Saskatchewan, for her assistance in preparing Au-coated Si wafers used as sample mounts for the C K-edge NEXAFS study. The NEXAFS research described in this work was performed at the Canadian Light Source (CLS), which is supported by NSERC, NRC, CIHR, and the University of Saskatchewan. We thank the SGM beamline scientists at the CLS, Robert Blyth and Tom Regier, for their assistance.

References

[1] M.-S. Rouet-Mayer, J. Ralambosoa, J. Philippon, Phytochemistry 29 (1990) 435–440.
[2] F.J. Hidalgo, R. Zamora, Grasa Aceites 51 (2000) 35–49.
[3] R. Zamora, F.J. Hidalgo, Crit. Rev. Food Sci. Nutr. 45 (2005) 49–59.
[4] S. Bittner, Amino Acids 30 (2006) 205–224.
[5] F.J. Stevenson, Humus Chemistry: Genesis, Composition, Reactions, John Wiley & Sons, New York, USA, 1994.
[6] J.-M. Bollag, J. Dec, P.M. Huang, Adv. Agron. 63 (1998) 237–266.
[7] P.M. Huang, in: M.E. Sumner (Ed.), Handbook of Soil Science, CRC Press, Boca Raton, FL, USA, 2000, pp. B302–B332.
[8] P.M. Huang, Adv. Agron. 82 (2004) 391–472.
[9] H. Shindo, P.M. Huang, Nature 298 (1982) 363–365.
[10] H. Shindo, P.M. Huang, Nature 308 (1984) 57–58.
[11] A. Jokic, H.-R. Schulten, J.N. Cutler, M. Schnitzer, P.M. Huang, Geophys. Res. Lett. 31 (2004) L05502.
[12] M.C. Wang, P.M. Huang, Soil Sci. 165 (2000) 934–942.
[13] M.C. Wang, P.M. Huang, Geoderma 112 (2003) 31–50.
[14] E.M. Majecher, J. Chorover, J.-M. Bollag, P.M. Huang, Soil Sci. Soc. Am. J. 64 (2000) 157–163.
[15] H. Shindo, P.M. Huang, Soil Sci. Soc. Am. J. 48 (1984) 927–934.
[16] M.C. Wang, P.M. Huang, Nature 323 (1986) 529–531.
[17] S. Hättenschwiler, P.M. Vitousek, Trends Ecol. Evol. 15 (2000) 238–243.
[18] T.R. Filley, G.D. Cody, B. Goodell, J. Jellison, C. Noser, A. Ostrofsky, Org. Geochem. 33 (2002) 11–124.
[19] S. Hättenschwiler, P.M. Vitousek, Biogeochemistry 64 (2003) 129–148.
[20] T.R. Fox, in: W.W. McFee, J.M. Kelly (Eds.), Carbon Forms and Functions in Forest Soils, Soil Science Society of America, Madison, WI, USA, 1995, pp. 43–62.
[21] A. Muscolo, M. Sidari, Plant Soil 284 (2006) 305–318.
[22] H.A. Anderson, W. Bick, A. Hepburn, M. Stewart, in: M.H.B. Hayes, P. MacCarthy, R.L. Malcolm, R.S. Swift (Eds.), Humic Substances II. In Search of Structure, Wiley-Interscience, Chichester, UK, 1989, pp. 223–253.
[23] N. Koivula, K. Hanninen, Chemosphere 44 (2001) 271–279.
[24] L.C. Maillard, C.R. Acad. Sci. 156 (1913) 148–149.
[25] R. Ikan, Y. Rubinsztain, A. Nissenbaum, I.R. Kaplan, in: R. Ikan (Ed.), The Maillard Reaction: Consequences for the Chemical and Life Sciences, John Wiley & Sons, Chichester, UK, 1996, pp. 1–25.
[26] P. Arafaioli, O.L. Pantani, M. Bosetto, G.G. Ristori, Clay Miner. 34 (1999) 487–497.
[27] M. Bosetto, P. Arafaioli, O.L. Pantani, Clay Miner. 37 (2002) 195–204.
[28] A. Jokic, Z. Zimpel, P.M. Huang, P.G. Mezey, SAR QSAR Environ. Res. 12 (2001) 297–307.
[29] A. Jokic, A.I. Frenkel, M.A. Vairavamurthy, P.M. Huang, Geophys. Res. Lett. 28 (2001) 3899–3902.
[30] A. Jokic, A.I. Frenkel, P.M. Huang, Can. J. Soil Sci. 81 (2001) 277–283.
[31] A. Jokic, M.C. Wang, C. Liu, A.I. Frenkel, P.M. Huang, Org. Geochem. 35 (2004) 747–762.
[32] A.G. Hardie, J.J. Dynes, L.M. Kozak, P.M. Huang, Ann. Environ. Sci. 1 (2007) 91–110.
[33] R.M. McKenzie, Miner. Mag. 38 (1971) 493–502.
[34] T.S.C. Wang, M.C. Wang, Y.L. Ferng, P.M. Huang, Soil Sci. 135 (1983) 350–360.
[35] J.I. Hedges, Geochim. Cosmochim. Acta 42 (1978) 69–79.
[36] L.M. Benzing-Purdie, J.A. Ripmeester, C.I. Ratcliffe, J. Agric. Food Chem. 33 (1985) 31–33.
[37] K. Taguchi, Y. Sampei, Org. Geochem. 10 (1986) 1081–1089.
[38] W.A. Jury, W.R. Gardener, W.H. Gardener, Soil Physics, Fifth ed., John Wiley & Sons, New York, USA, 1991.
[39] M.B. McBride, Environmental Chemistry of Soils, Oxford University Press, London, UK, 1994.
[40] D. Gan, S.I. Kotob, D.S. Walia, Ann. Environ. Sci. 1 (2007) 11–15.
[41] Y. Chen, N. Senesi, M. Schnitzer, Soil Sci. Soc. Am. J. 41 (1977) 352–358.
[42] R.S. Swift, in: D.L. Sparks (Ed.), Methods of Soil Analysis. Part 3. Chemical Methods, Soil Science Society of America, Madison, WI, USA, 1996, pp. 1018–1020.
[43] T. Regier, J. Paulsen, G. Wright, I. Coulthard, K. Tan, T.K. Sham, R.I.R. Blyth, AIP Conference Proceedings, vol. 879, 2007, pp. 473–476.
[44] B. Watts, L. Thomsen, P.C. Dastoor, J. Electron Spectrosc. 151 (2006) 105–201.
[45] A.P. Hitchcock, C. Morin, X. Zhang, T. Araki, J.J. Dynes, H. Stover, J.L. Brash, J.R. Lawrence, G.G. Leppard, J. Electron Spectrosc. 144–147 (2005) 259–269.
[46] L.A.J. Garvie, A.J. Craven, Phys. Chem. Miner. 21 (1994) 191–206.
[47] J. Boese, A. Osanna, C. Jacobsen, J. Kirz, J. Electron Spectrosc. 85 (1997) 9–15.
[48] R.M. McKenzie, in: J.B. Dixon, S.B. Weed (Eds.), Minerals in Soil Environments, Soil Science Society of America, Madison, WI, USA, 1989, pp. 439–465.
[49] R.M. Potter, G.R. Rossman, Am. Miner. 64 (1979) 1199–1218.
[50] O. Novotny, K. Cejpek, J. Velisek, Czech. J. Food Sci. 26 (2008) 117–131.
[51] S.P. Wolff, in: R. Ikan (Ed.), The Maillard Reaction. Consequences for the Chemical and Life Sciences, John Wiley & Sons, Chichester, UK, 1996, pp. 73–88.
[52] W.L. Lindsay, Chemical Equilibria in Soils, John Wiley & Sons, New York, USA, 1979.
[53] M.C. Wang, P.M. Huang, Sci. Total Environ. 62 (1987) 435–442.
[54] M.C. Wang, P.M. Huang, in: J. Drozl, S.S. Gonet, N. Senesi, J. Webber (Eds.), Proceedings of the 8th Conference of the International Humic Substances Society, Wroclaw, Poland, 1997, pp. 59–65.
[55] M.C. Wang, C.H. Lin, Soil Sci. Soc. Am. J. 57 (1993) 88–93.
[56] A.T. Stone, Environ. Sci. Technol. 21 (1987) 979–988.
[57] V.V. Mossine, G.V. Glinsky, M.S. Feather, Carbohydr. Res. 262 (1994) 257–270.
[58] K. Lourvanij, G.L. Rorrer, Appl. Catal. A 109 (1994) 147–165.
[59] L.J.W. Haffenden, V.A. Yaylayan, J. Agric. Food Chem. 53 (2005) 9742–9746.
[60] G. Furlani, F. Pagnanelli, L. Toro, Hydrometrics 81 (2006) 234–240.
[61] J.M. Gonzalez, D.A. Laird, Clays Clay Miner. 54 (2006) 38–44.
[62] S.G. Urquhart, H. Ade, J. Phys. Chem. B 106 (2002) 8531–8538.
[63] O. Dhez, H. Ade, S.G. Urquhart, J. Electron Spectrosc. 128 (2003) 85–96.
[64] R.R. Cooney, S.G. Urquhart, J. Phys. Chem. B 108 (2004) 18185–18191.
[65] A.P. Hitchcock, D.C. Mancini, Gas-phase Core Excitation Database, 2004.

[66] S.C.B. Myneni, in: P.A. Fenter, M.L. Rivers, N.C. Sturchio, S.R. Sutton (Eds.), Applications of Synchrotron Radiation in Low-temperature Geochemistry and Environmental Sciences, Mineralogical Society of America, Washington, DC, USA, 2002, pp. 485–558.
[67] J.T. Francis, A.P. Hitchcock, J. Phys. Chem. 96 (1992) 6598–6610.
[68] R.M. Silverstein, F.X. Webster, D. Kiemle, Spectrometric Identification of Organic Compounds, John Wiley & Sons, New York, USA, 2004.
[69] N. Aktas, N. Sahiner, O. Kantoglu, B. Salih, A. Tanyolaç, J. Polym. Environ. 11 (2003) 123–128.
[70] H.W. van der Merel, H. Beutelspacher, Atlas of Infrared Spectroscopy of Clay Minerals and their Admixtures, Elsevier, Amsterdam, The Netherlands, 1976.
[71] R.A. Nyquist, R.O. Kagel, Infrared Spectra of Inorganic Compounds, Academic Press Inc., Orlando, FL, USA, 1971.
[72] I. Christl, R. Kretzchmar, Environ. Sci. Technol. 41 (2007) 1915–1920.
[73] J.L. Bose, A.B. Foster, M. Stacey, J.M. Webber, Nature 184 (1959) 1301–1302.
[74] M.S. Feather, J.S. Harris, Adv. Carbohydr. Chem. Biochem. 28 (1973) 161–224.